ADVANCED MATERIALS TECHNOLOGIES
www.advmattechnol.de

Stretchable, Breathable, and Washable Fabric Sensor for Human Motion Monitoring

*Lina Sanchez-Botero, Anjali Agrawala, and Rebecca Kramer-Bottiglio**

Wearable strain sensors for movement tracking are a promising paradigm to improve clinical care for patients with neurological or musculoskeletal conditions, with further applicability to athletic wear, virtual reality, and next-generation game controllers. Clothing-like wearable strain sensors can support these use cases, as the fabrics used for clothing are generally lightweight and breathable, and interface with the skin in a manner that is mechanically and thermally familiar. Herein, a fabric capacitive strain sensor is presented and integrated into everyday clothing to measure human motions. The sensor is made of thin layers of breathable fabrics and exhibits high strains (>90%), excellent cyclic stability (>5000 cycles), and high water vapor transmission rates (≈50 g/h m^2), the latter of which allows for sweat evaporation, an essential parameter of comfort. The sensor's functionality is verified under conditions similar to those experienced on the surface of the human body (35°C and 90 ± 2% relative humidity) and after washing with fabric detergent. In addition, the fabric sensor shows stable capacitance at excitation frequencies up to 1 MHz, facilitating its low-cost implementation in the Arduino environment. Finally, as a proof of concept, multiple fabric sensors are seamlessly integrated with commercial activewear to collect movement data. With the prioritization of breathability (air permeability and water vapor transmission), the fabric sensor design presented herein paves the way for future comfortable, unobtrusive, and discrete sensory clothing.

1. Introduction

In recent years, a growing interest in wearable electronic devices has turned continuous health monitoring into an achievable and mainstream concept, with revolutionary implications for human health, safety, and performance. While wearable commercial devices currently allow users to monitor physiological data such as heart rate, skin conductance, and respiration patterns,[1] there is still a need for noninvasive human motion monitoring systems capable of capturing the body strains involved in everyday activities.

In situ collection of human motion data is crucial for advancing the current state of a broad range of disciplines including human–robot interactions,[2] virtual reality,[3,4] sports performance,[5,6] and personalized health monitoring [7] and rehabilitation.[8] Most commonly, human motion data is collected via use of optical, electromagnetic, and inertial measurement unit (IMU) motion capture systems.[9] Although optical motion capture systems—consisting of multiple cameras oriented around a subject—are broadly considered the gold standard for high accuracy,[10] these systems are susceptible to measurement errors and loss of analyzable data due to occluded lines of sight.[9,11] Such setups limit the spatial volume of the analysis and necessitate controlled laboratory environments.[9,10,12] In contrast, electromagnetic motion capture systems employ sensors that provide measurements without requiring lines of sight.[9,13] However, this method is still limited to use in controlled settings because electromagnetic interference from the surrounding environment can lead to measurement errors.[9,13] Like electromagnetic motion capture sensors, IMUs can be mounted onto the subject and provide measurements using only the onboard gyroscope and accelerometer. While the use of IMUs is not limited to controlled laboratory settings, they exhibit positional drift in long-term measurements[10] and are made of rigid components, which limit user comfort.

The development of soft strain sensors has shown promise for circumventing the existing challenges of traditional motion capture systems and enabling unobtrusive integration of human motion monitoring. Typically, such soft strain sensors employ conductive composites with fillers such as carbon black,[14,15] carbon nanotubes,[16–18] metallic nanoparticles,[19] silver nanowires,[3,20] graphene,[21,22] liquid metals,[23–26] and/or ionic fluids[27,28] to create electrodes. Silicone-based elastomers such as polydimethylsiloxane (PDMS), Ecoflex, and Dragon Skin[29] usually serve as both insulating host materials and highly stretchable substrates. The use of such compliant materials allows soft sensors to conform to curvilinear surfaces (e.g., elbows, knees) and withstand the everyday skin deformations of human joints (in the range of 40%–55% strain[30–33]) without impeding natural motion. Most soft strain sensors transduce uniaxial mechanical deformation

L. Sanchez-Botero, A. Agrawala, R. Kramer-Bottiglio
School of Engineering & Applied Science
Yale University
17 Hillhouse Ave, New Haven, CT 06520, United States
E-mail: rebecca.kramer@yale.edu

The ORCID identification number(s) for the author(s) of this article can be found under https://doi.org/10.1002/admt.202300378

DOI: 10.1002/admt.202300378

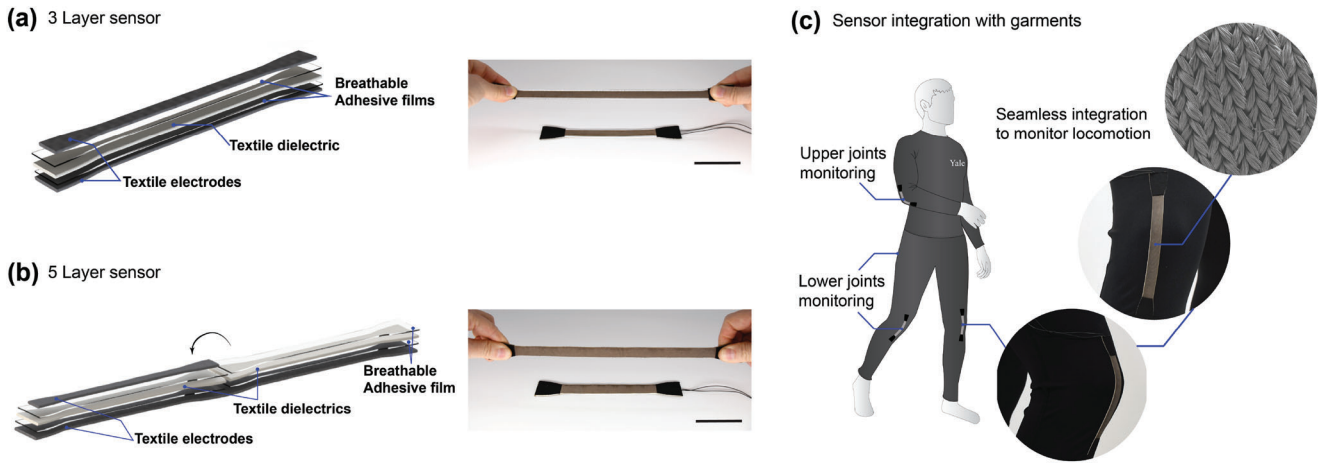

Figure 1. Fabric sensor overview. a) three-layer construction. b) five-layer construction. Scale bars: 54 mm. c) Sensors integrated into garments for human motion monitoring.

into a change in either electrical resistance or capacitance. Resistive strain sensors have demonstrated higher sensitivities than capacitive strain sensors overall,[14,29,32] but many also show limited electromechanical robustness, hysteresis, and low sensing stability due to crack formation and mechanical damage at high strains.[33] Since the sensor response of most capacitive sensors relies on the overlapping area of electrodes, capacitive sensors generally show more linear and stable behavior,[32] both of which are particularly important in human motion monitoring.

Although there are many capacitive strain sensors in existing literature,[29,33,34] including previous works from our lab,[35–37] there remain several key ongoing challenges in the field regarding breathability, maximum measurement frequency, and sensor-garment integration. Here, we present a wearable capacitive sensor that addresses these identified limitations.

First, despite the prevalence of elastomer-based sensors in the literature, such sensors compromise thermophysiological and skin sensorial comfort due to the low air permeability and water vapor transmission of elastomers. Recent works have started exploring the use of fabrics to improve sensor comfort. Prior work by Atalay et al.[38] introduced a soft parallel-plate capacitor constructed using conductive fabric as electrodes and a silicone layer as the dielectric material. Although this sensor uses fabric as the outer exposed (conductive) layers, the internal silicone dielectric layer limits the overall breathability of the sensor. Another capacitive sensor by Park et al.[39] uses silicone to bind fabric layers such that fabrics serve as both the electrode and dielectric materials. In both of these works, as well as most wearable electronics and sensor literature, the breathability of the sensor materials was not characterized. To maximize wearer comfort and safety, and encourage real-world usage, we sought to create a reliable strain sensor made of entirely conductive and non-conductive fabrics bound together with thin films of breathable thermoplastic fabric adhesive (**Figure 1**a,b).

Second, prior work has established that electrode resistance can affect the maximum frequency at which capacitance can be accurately measured, with characteristic frequencies around 5 kHz.[36] In this work, we demonstrate stable capacitance measurements up to 1 MHz, such that our sensor data can be easily read using standard Arduino hardware. The fidelity of the sensor response at high frequencies indicates its suitability for broader translation into soft robotics applications.

Third, our fabric sensor can be directly embedded into commercial activewear, even using the garments as the dielectric layer of the sensors, thus overcoming existing challenges of bulky attachment modes and sensor detachment and/or slippage.[40,41]

By using fabrics and porous layers that offer a unique combination of flexibility, stretchability, and breathability, our aim is to prioritize sensor wearability and user tactile comfort (as measured by air permeability and water vapor transmission) in a way that existing elastomer-based sensors do not. In this paper, we characterize sensor performance using three common fabrics—cotton, polyester, and nylon—as the dielectric materials to demonstrate the respective advantages of each. We further report the sensor's cyclic stability, frequency dependence, electromechanical response to temperature and humidity, and washability. Along with its functional benefits, the textile sensors are fabricated using a simple, highly reproducible, and low-cost stacked assembly method, which allows their seamless integration into commercial clothing to facilitate the collection of reliable human motion data.

2. Results and Discussion

2.1. Sensor Overview

The capacitive strain sensors shown in Figure 1a,b consists of conductive fabric electrodes separated by dielectric fabric layers. Each layer is stacked and affixed with breathable adhesive film. Flexible wires are used to interface the sensors with external data acquisition electronics (Arduino Pro mini and MPR121 Adafruit breakout circuit). We tested both three- and five-layer sensor configurations (Figure 1a,b; sensor dimensions shown in Figure S1). In the five-layer configuration, the external electrode is connected to ground, which reduces parasitic capacitance and shields the sensor, therefore making the device more suitable for contact with human skin. The characteristics of the constituent sensor materials and the straightforward fabrication process

allow seamless sensor integration into existing knitted garments. The result of this integration is a sensory garment capable of monitoring the movement of body joints (Figure 1c).

2.2. Air Permeability and Water Vapor Transmission Characterization

Comfort is one of the most critical components of modern wearable devices, however, this feature is often overlooked in the development of new wearable sensors. For fabrics, tactile and thermophysiological comfort is related to the breathability of the material.[42] Thus, to evaluate the breathability of our sensor, we tested the air permeability and water vapor transmission rate (WVTR) of the sensor's constituent fabrics both with and without thermoplastic adhesive (**Figure 2**a,b). Our sensors are constructed using knit fabrics—a medical-grade conductive nylon for the electrodes, and three different fabrics for the dielectric layers: nylon, polyester, and cotton. Air permeability was measured according to the ASTM 737–18 procedure,[43] which determines the volume rate of air flow per unit area of fabric. Both the conductive fabric (Figure 2c) and the dielectric nylon fabric (Figure 2d) exhibit a warp-knit tricot structure (Figure S2, Supporting Information), with air permeability values of 2253.3 and 414 l/m^2s, respectively. Although both the conductive and the dielectric nylon fabrics have the same knit structure, the dielectric nylon fabric exhibits a tighter knit (and thus a lower air permeability) relative to the more open structure of the conductive fabric. In contrast, the polyester (Figure 2e) and cotton (Figure 2f) dielectric fabrics exhibit a weft-knit jersey structure (Figure S2, Supporting Information) with air permeability values of 183 and 439 l/m^2s, respectively. As polyester is the heaviest and thickest of the fabrics we tested, it exhibits the lowest air permeability (Figure S2 and Table S1, Supporting Information). Additional fabric characteristics such as fiber hydrophilicity,[44] yarn count,[45] weave or knit structure,[46–48] fabric thickness,[49,50] and fabric porosity[51] have also been shown to affect air permeability and water vapor transmission.

We refer to fabrics coated with the thin film adhesive (a thermoplastic polyurethane fabric tape; morphology shown in Figure S3, Supporting Information) as laminated fabrics. Once adhered to the fabrics, the adhesive visually presents as a porous membrane (third column in Figure 2c–f). As a result, the air permeability of the laminated fabrics is reduced compared to their bare fabric counterparts (Figure 2a). On average, the air permeability of laminated nylon and polyester is 163 and 129 l/m^2s, respectively. These values constitute a respective reduction by ≈ 60% and ≈ 30% relative to the bare samples. Laminated cotton exhibits a reduction in permeability of only ≈ 15%. In contrast, laminated conductive nylon exhibits a reduced permeability of ≈ 97.2%, which is attributed to the reduced porosity shown in Figure 2c.

Although the air permeability of the laminated fabrics was reduced relative to the bare fabrics, the laminated dielectric fabrics all showed air permeabilities greater than 100 l/m^2s, which falls within the range of normal clothing breathability as reported by Havenith et al.[52] On average, the laminated conductive fabric showed an air permeability slightly less than this value (62 l/m^2s). However, the order of attachment of the adhesive to the fabric likely plays a role in the porosity of the fabric-bonded adhesive and air permeability of the overall composite. Thus, attaching the adhesive to the dielectric fabric first enables the air permeability of composite layers to be greater than 100 l/m^2s.

Water-vapor permeability is another key physical property of fabrics affecting breathability since the loss of water vapor is crucial for the wearer's thermal equilibrium and physiological comfort.[53] Measurements show high WVTRs for all the bare fabrics with average values between 45 and 51 $g/h\ m^2$. All laminated fabrics exhibit similarly high WVTR, with average values between 38 and 41 $g/h\ m^2$ (Figure 2b). The laminated fabrics behave as porous membranes with WVTRs higher than the rate of transepidermal water loss (TEWL) of adult skin under normal conditions (5–10 $g/h\ m^2$) and within the range of TEWL during sweating (6–66 $g/h\ m^2$). Our samples also have WVTRs higher than those of non-porous 8 μm[54] and highly porous (45%) 40 μm[55] films of polydimethylsiloxane (5–6 and 20.3 $g/h\ m^2$, respectively), which are elastomers commonly used in wearable devices. Therefore the data cumulatively suggest that fabric lamination with the adhesive film has a minimal blocking effect on moisture permeability.

2.3. Electromechanical Characterization

Although the three-layer configuration for capacitive sensors is the most widely used in electrical and robotic applications, the five-layer configuration is most suitable for wearable applications in contact with the human skin. In the five-layer configuration, the external electrode acts as an active shield when connected to ground, mitigating parasitic and environmental interference factors and resulting in a high fidelity signal. In the three-layer configuration, while operational in wearable applications, direct skin contact with the signal electrode may lead to shorting and losses in the electrical signal. We evaluated the strain sensing performance of the three- and five-layer sensors with nylon, polyester, or cotton dielectric layers by monitoring the relative change in capacitance, $\Delta C/C_0$, during uniaxial tensile strain, ϵ. While the relation between capacitance and strain monotonically increases in all cases, we observed a degree of non-linearity in the measured curves (**Figure 3**a–c for five-layer sensors; Figure S4a–c, Supporting Information, for three-layer sensors). It is important to note that the relative change in the capacitance response to strain for both three- and five-layer sensors are comparable (see the curves overlap in Figure S5, Supporting Information), showing that increasing the area of one electrode in the five-layer configuration seems not to affect the sensor response to deformation. The nonlinearity in the relative capacitance of our sensors can be explained by changes in the mesostructure of the fabric dielectric layer under strain, such as reduction of the porosity,[56] partial alignment of the fibers,[57] and compressive deformation.[58,59] For the purpose of our analysis, we define three linear strain regions: $\epsilon < 25\%$, $25\% < \epsilon < 50\%$, $\epsilon > 50\%$.

The sensitivity, S, in each strain region is defined by the linear fit slope: $\frac{\delta(\Delta C/C_0)}{\delta\epsilon}$. Similar segmented linearity analyses have been used in nonlinear capacitance responses to deformation in pressure sensors with highly structured dielectric layers.[60–62] Figure 3a–c shows that all three sensor types increase in sensitivity with increasing strain. The polyester sensors exhibit the

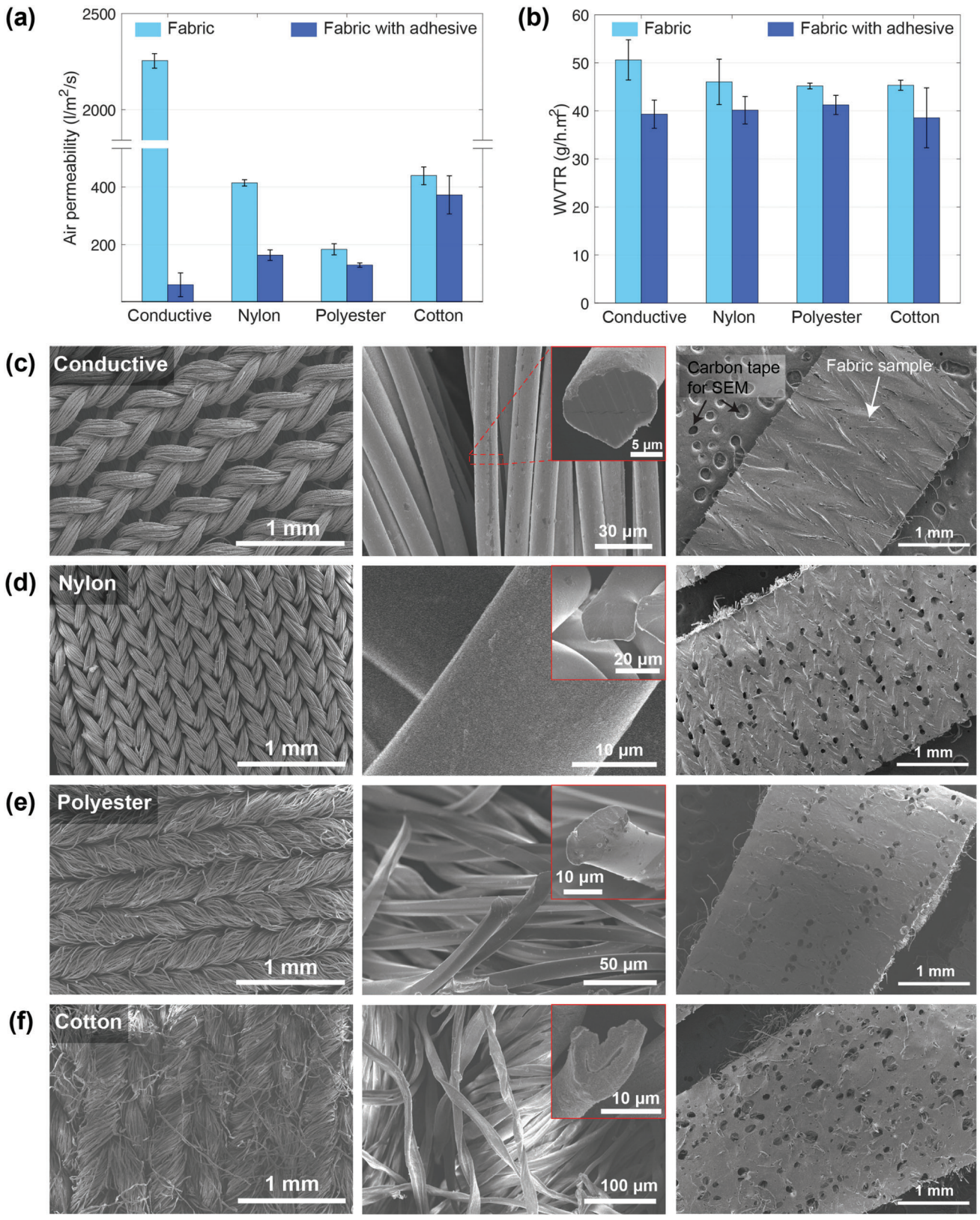

Figure 2. Constituent sensor material breathability and morphological characterizations. a) Air permeability and b) water vapor transmission rate of bare and laminated fabrics (i.e., fabrics coated with the adhesive). An average of three samples is shown for each. c–f) SEM images of (c) conductive nylon, (d) nylon, (e) polyester, and (f) cotton. Columns from left to right: the front side of the bare fabrics, fiber morphologies, and laminated fabrics.

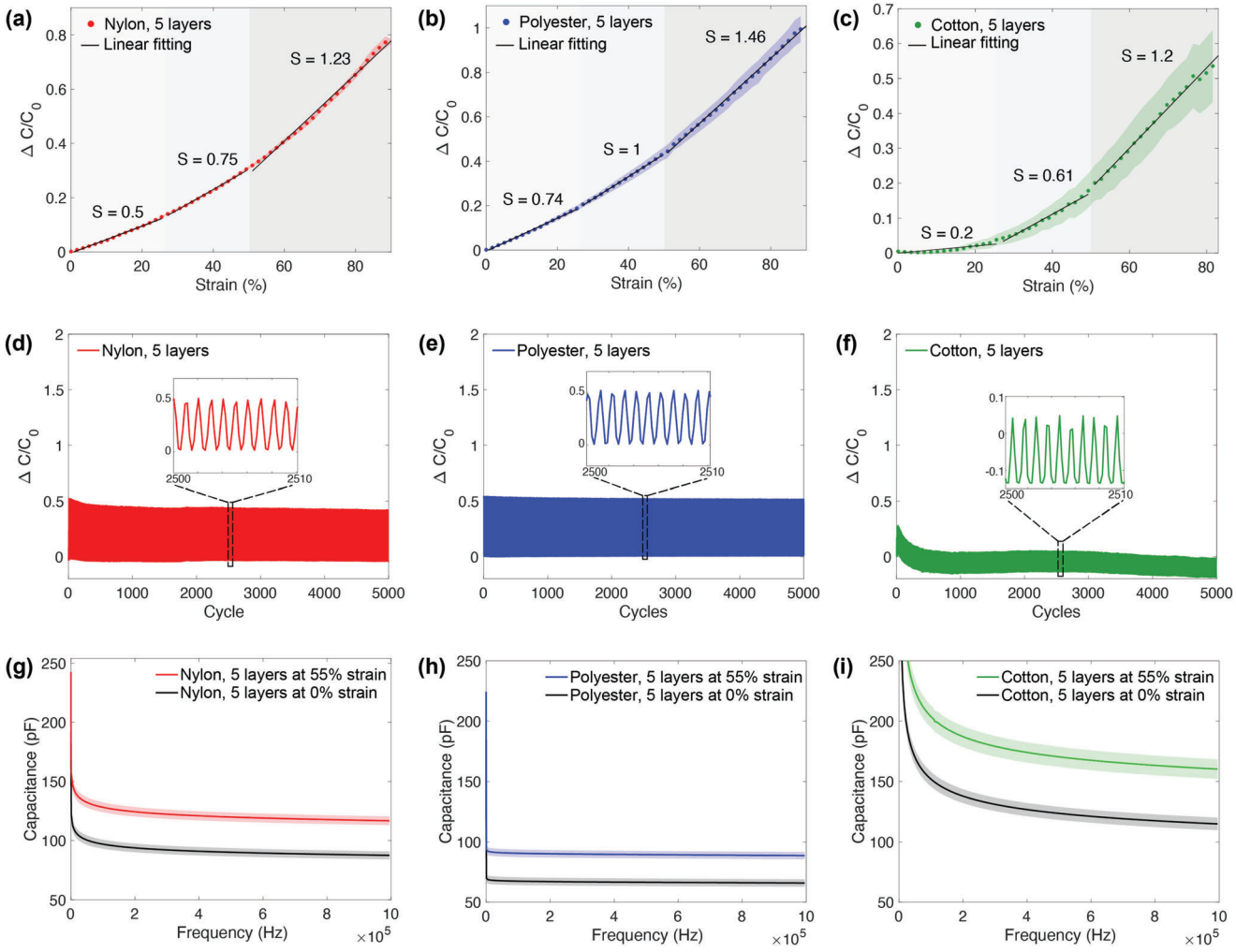

Figure 3. Electromechanical characterizations of five-layer fabric sensors. a–c) Average relative change in capacitance as a function of strain for five sensors with dielectric (a) nylon, (b) polyester, and (c) cotton. Three sensitivity regimes are shown. d–f) 5000 strain cycles to ≈ 60% for a representative sensor with dielectric (d) nylon, (e) polyester, and (f) cotton. g–i) Average change in capacitance as a function of frequency for five sensors with dielectric (g) nylon, (h) polyester, and (i) cotton.

highest sensitivity ($S = 0.74$ for $\epsilon < 25\%$, $S = 1$ for $25\% < \epsilon < 50\%$, $S = 1.46$ for $\epsilon > 50\%$). The nylon sensors exhibit a similar, though slightly lessened, sensitivity ($S = 0.5$ for $\epsilon < 25\%$, $S = 0.75$ for $25\% < \epsilon < 50\%$, $S = 1.23$ for $\epsilon > 50\%$). The cotton sensors exhibit the lowest sensitivity ($S = 0.2$ for $\epsilon < 25\%$, $S = 0.61$ for $25\% < \epsilon < 50\%$, $S = 1.2$ for $\epsilon > 50\%$). Both the nylon and polyester sensors exhibit sensitivity values that are comparable to prior textile-inclusive capacitive sensors. For example, Atalay et al.[38] report a sensitivity value of 1.23 up to 100% strain, and Geng et al.[63] report a sensitivity of 0.7 up to 30% strain. The suppressed sensitivity of the cotton sensors can be explained by several factors. Cotton is the least elastic of the dielectric fabrics, with a spandex percentage of only 5%, compared to 20% for nylon and polyester fabrics. Although the thicknesses of the cotton and nylon dielectric fabrics are comparable, the weight of the cotton fabric is the lowest among the dielectric fabrics, with fewer courses and wales per inch (see Table S1, Supporting Information). Thus, the reduced sensitivity of the cotton sensors is likely a combined result of the fiber content, fabric thickness, and the dielectric properties of the cotton fibers. While dielectric properties of fabrics are mainly defined by the fiber's polymer composition, in our case, nylon, polyester, and cotton, secondary parameters, such as yarn structure and fabric construction, have also shown substantial effects on the fabric's dielectric behavior. For further reading, we refer readers to a recent review on fabric dielectric properties.[64]

We note here that segmented linearity is one approach to modeling the overall non-linear capacitance response to deformation. However, continuous non-linear models may be helpful to further predict sensor performance for a wide range of sensor designs. As it is known that the Poisson's ratio of elastic and porous systems is dependent on strain,[58] we speculate that there further exists a dependence between the dielectric properties of the sensors to strain, as the fabric's microstructure undergoes compression during stretch inducing changes in the effective dielectric constant. Similar results have been observed in microstructure capacitive pressure sensors where the effective dielectric constant changes with the displaced air in the dielectric layer upon compression.[60,61,65] By introducing these two

strain-dependent parameters, Poisson's ratio and effective dielectric constant, we propose a non-linear empirical model, given in Note S1 and Equation S19 (Supporting Information). The non-linear model predictions are in agreement with experimental data for nylon and polyester sensors, thereby providing a first validation of the changes in capacitance for porous dielectric materials such as fabrics, even under different environmental conditions (see Figure S17 and Table S2, Supporting Information). However, further investigation is required to understand the capabilities and robustness of the proposed empirical model.

The stress-strain behavior of the three- and five-layer sensors with nylon, polyester, or cotton dielectric layers is shown in Figure S6 (Supporting Information). The five-layer nylon and polyester sensors showed maximum stresses of 0.80 and 1.11 MPa at 85% and 87% strain, respectively, while both the three- and five-layer cotton sensors exhibited stresses of ≈2 MPa at 82% strain. The observed mechanical responses are comparable to those of elastomeric strain sensors[66,67] and their constituent materials.[68]

The cyclic stability of the sensors was assessed via 5000 loading cycles with applied strain between 5% and 60%. All sensor types completed the test without failure (Figure 3d,e for five-layer sensors; Figure S7, Supporting Information, for three-layer sensors). The insets in Figure 3d,e provide a detailed view of the capacitance changes of representative sensors during tensile stretching for ten consecutive cycles (from the 2500th to the 2510th cycles). Repeatability and reliability can be observed for the polyester sensor, which shows a stable relative change in capacitance of $\Delta C/C_0 \approx 0.43\%$ at ≈ 60% strain (Figure 3e). The nylon sensor exhibited a small drift during the cyclic test with $\Delta C/C_0 \approx 0.51\%$ at ≈ 60% strain during the first cycle and $\Delta C/C_0 \approx 0.45\%$ at ≈ 60% strain for the 5000th cycle (Figure 3d). The cotton sensor had a short transient regime during the cyclical testing, reaching a stable absolute value of ≈ 0.2% for $\Delta C/C_0$ after several hundred loading cycles. This observed settling may be related to the slower gradual rearrangement of the cotton fabric network during the beginning cycles.[69] The spandex percentage in the cotton fabric is only 5%, compared to 20% for nylon and polyester fabrics, resulting in more plastic deformation in the cotton sensors (see Figure S8, Supporting Information). Additionally, the highly hygroscopic nature of cotton may further affect its mechanical[70,71] and dielectric[64,72] properties, as fiber rearrangement and deformation induce changes in exposed surface area during cyclic testing.

The dependence between capacitance and excitation frequency of the manufactured sensors was investigated in the frequency range from 20 Hz to 1 MHz at room temperature (Figure 3g–i). The measured capacitance of both unstrained (0%) and strained (55%) sensors rapidly decreases at low frequency values, which can be explained by the dielectric dispersion of the fabrics. In polar polymers such as cotton, nylon, and polyester, at high frequencies of the applied electric field, the electric dipoles do not have time to align before the field changes direction, leading to a decrease in permittivity and, therefore, capacitance.[64] As the applied frequency increases, the capacitance response for nylon and polyester sensors becomes almost independent of frequency, while for cotton sensors a monotonic decrease of the capacitance as a function of frequency was observed. At the same relative humidity (RH) conditions, cotton will have a higher moisture content than nylon and polyester fabrics due to its hygroscopicity.[70,71] The higher content of bound water in cotton may further affect dielectric permittivity,[64,72] resulting in a more monotonic frequency sweep curve.

The performance metrics of wearable polymer-based[32] and textile-based[33] strain sensors have been rigorously summarized in recent literature reviews. Herein, we provide the performance results necessary to benchmark our textile sensor using the comparison tables and references included in these reviews. Relative to the two polymer-based capacitive sensors summarized by Souri, et al.,[32] our sensor boasts a favorable response time though less favorable gauge factor, stretchability, and linearity. Further, we introduce air permeability and water vapor transmission rate as new metrics that have not been previously reported for wearable sensors. Electromechanical characterizations relating to response time (Figure S9, Supporting Information), hysteresis (Figure S10, Supporting Information), and strain rate dependency (Figure S11, Supporting Information) are shown in Supporting Information.

2.4. Electromechanical Dependence on Temperature and Humidity

We investigated the effects of temperature and humidity on the electromechanical response of our nylon and polyester five-layer sensors using our materials testing system (Instron 3345) outfitted with an environmental chamber (ETS, Model 5500-8485). The nylon and polyester sensors were chosen for further characterization over the cotton sensors due to their higher sensitivity, greater cyclic stability, and reduced frequency dependence. The sensors were tested in three conditions: 1) ambient humidity (51 ± 3% Relative Humidity (RH)) and room temperature (RT) (24 ± 1°C); 2) high humidity (90 ± 2% RH) and RT; and 3) high humidity (90 ± 2% RH) and high temperature (35 ± 1°C). After conditioning the sensors in each temperature and humidity setting for at least 3 h, the sensors were manually pre-stretched to remove any Mullins effect. Sensors were then strained to 55% of their new gauge length after the manual pre-stretch. Both sensor types showed a monotonically increasing relative capacitance with strain in all conditions (**Figure 4**a,b). Thus, our sensors remain functional in high moisture settings without requiring additional silicone encapsulation that would increase their weight, hinder their integration into clothing, and result in the loss of breathability and fabric feel.

While retaining function, the sensitivity of the sensors was impacted by the environmental conditions (Figure S12, Supporting Information). The hydrophobic and hygroscopic properties of the fabrics used as dielectric layers in the sensors resulted in different electrical responses with changing humidity. At higher relative humidities, fibers will absorb moisture from the environment and have higher moisture contents, filling air voids within the fibers and in the porous fabric structure. In this process, the relative permittivity of the fabric increases because the permittivity of water ($\epsilon_r = 78$ at 2.45 GHz and 25°C)[73] is much higher than that of air ($\epsilon_r \approx 1$).[73,74] This effect is seen in the overall increase in sensor capacitances at higher humidity levels (Figures S13 and S14, Supporting Information). At 0% strain, the increase in sensor capacitance of the five-layer nylon sensors at higher humidity

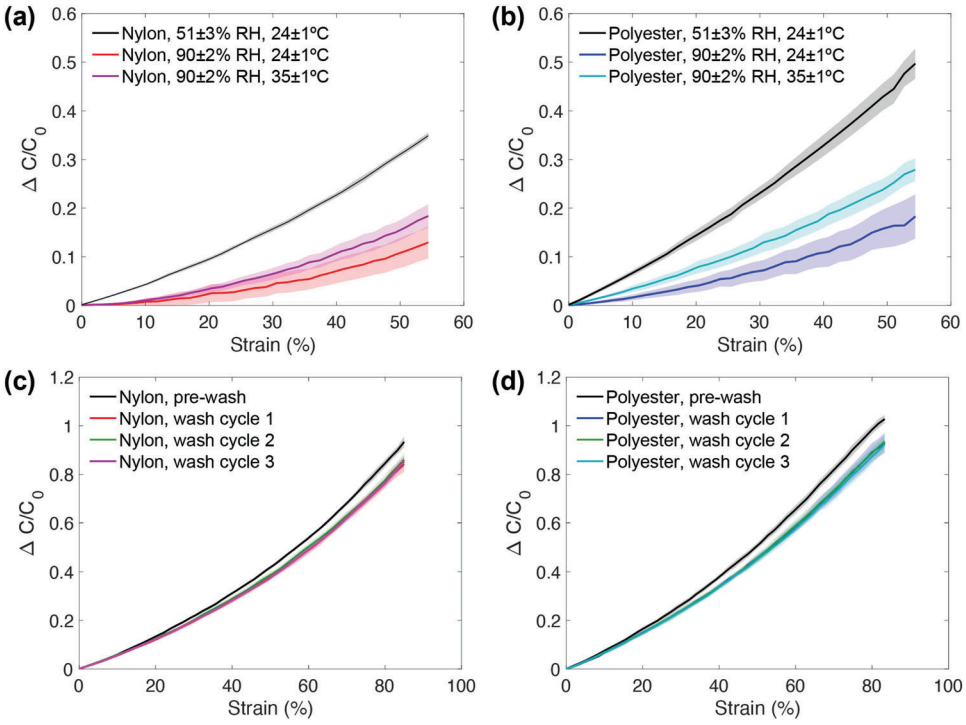

Figure 4. Effect of temperature, humidity, and washing on the electromechanical response of five-layer sensors. a,b) Average relative change in capacitance as a function of strain, under varying temperatures and humidities, for five sensors with dielectric (a) nylon and (b) polyester. c,d) Effect of washing on the electromechanical response of five sensors with dielectric (c) nylon and (d) polyester.

(≈50 pF) is greater than that of the five-layer polyester sensors (≈24 pF), reflecting the greater hydrophobicity and lower moisture uptake of polyester relative to nylon. Within the tested strain range, it is also evident that the magnitude of capacitance change (ΔC) is greatest in ambient humidity for both nylon and polyester sensors, further contributing to the reduced sensitivity of the sensors at high humidity (Figure S13, Supporting Information). Sensor capacitance showed more susceptibility to humidity than temperature (Figure S15, Supporting Information). However, we also observed an increase in sensor sensitivity at higher temperatures. We attribute this increased sensitivity to increased drying of the sensors at higher temperatures, which would reduce their water uptake and partially counteract the effects of higher humidity. Further investigation is needed to decouple the effects of these variables from strain to enable robust and reliable motion tracking.

The sensors were also washed with fabric detergent, then dried and tested three times in room conditions (24 ± 1°C and 51 ± 3%). The electromechanical response of both the nylon and polyester five-layer sensors showed a slight decrease in sensitivity after the initial wash cycle, but no noticeable changes after repeated wash cycles (Figure 4c,d). Previous literature has used SEM imaging to verify that washing silver nanoparticle-coated knitted fabrics reduces the concentration of conductive nanoparticles on fiber surfaces, resulting in decreased conductivity.[75] Thus, the mechanical and frictional forces involved in the first wash cycle may have led to a decrease in the conductivity of the electrode fabric and a subsequent drop in the sensitivity of the sensors. During the washing process, the fibers in the fabric layers also experienced axial and transverse swelling. During drying, the contact network between fibers may have changed, affecting the tightness of the knit structures and the permittivity properties of the dielectric fabrics. Nevertheless, the repeatability of sensor performance with repeated washes supports the hygienic reusability of the sensor.

2.5. Wearable Applications of the Capacitive Strain Sensor

Monitoring human activity is a key component of advancing the promising fields of human-machine interactions (HMI) and personal healthcare. The stretchability, signal fidelity, and permeability of our capacitive strain sensors allowed monitoring of large-range human motions by placing six sensors on each of the main human joints—elbows, hips, and knees. The six sensors were seamlessly integrated into commercial, nylon-based compression garments using the same breathable adhesive used in the sensor construction (described further in §4.6). The garment itself served as one of the dielectric layers in the five-layer sensor structure, with the second dielectric layer made of an additional layer of nylon (**Figure 5a**). The volunteer wearing the sensory garment was asked to perform different compound body movements such as squats, sit-to-stand, and step-ups. The distinct motions of the joints were unambiguously reflected in the capacitance changes of all six sensors. The measurements were also reproducible, without any obvious loss of the capacitive signal during repeated movements. For instance, when the volunteer performed a set of 10 squats, the capacitive

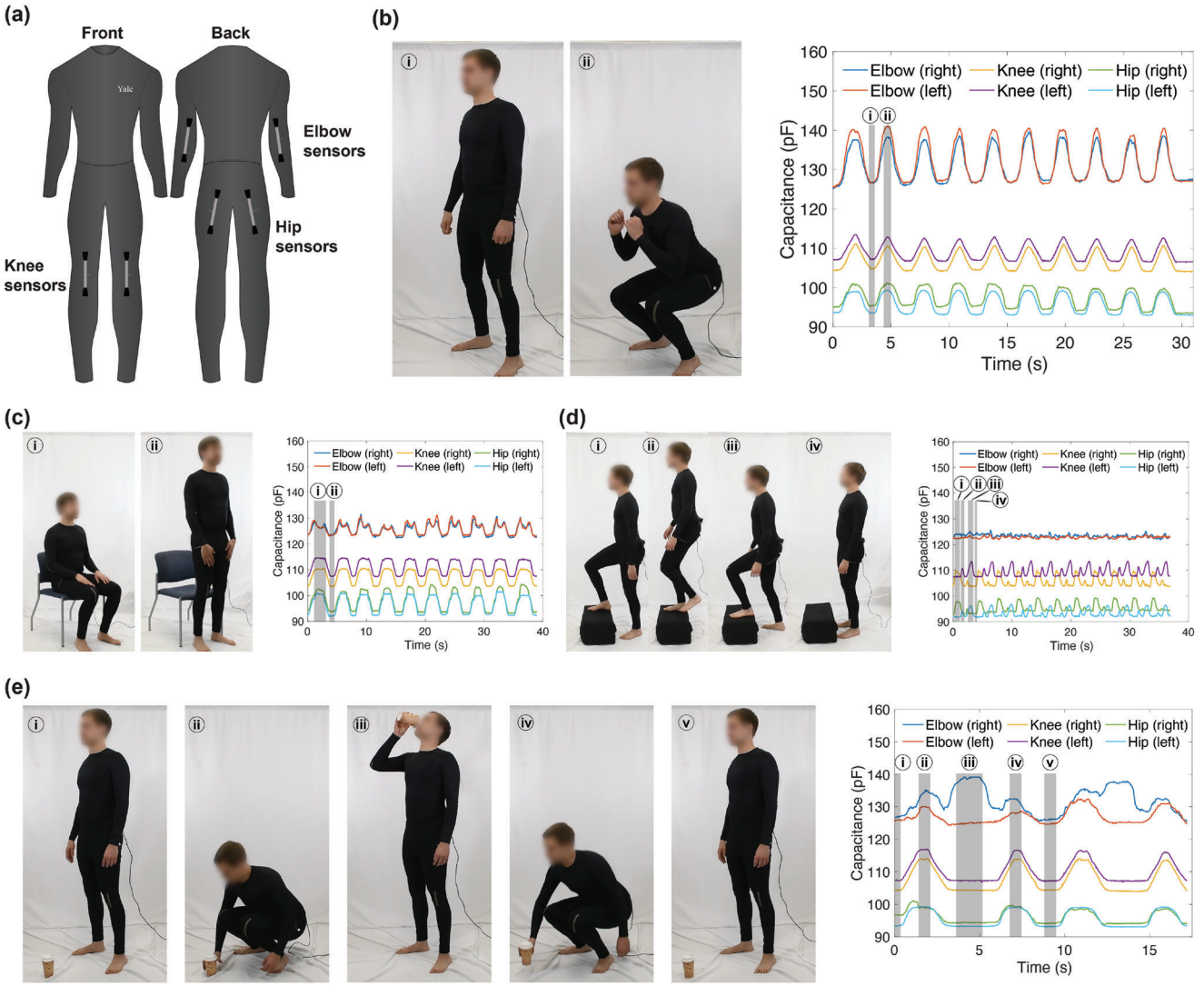

Figure 5. Sensory smart garment capable of monitoring the movement of body joints. a) Sensor placement on the knees, elbows, and hips of the garments. Photographs and capacitance responses of the sensors during the following human motions: b) squats (10 cycles), c) sit–to–stand cycles (10 cycles) d) step–ups (10 cycles) and e) retrieving an object from the floor (2 cycles).

response of the sensors exhibited several peaks (Figure 5b,ii) and valleys (Figure 5b,i) in the plot corresponding to the bending motions of the six joints under monitoring. The capacitive response of all body-mounted sensors increased when the wearer was gradually squatting down, and remained nearly constant as long as the joints remained static (see Video S1, Supporting Information).

Another validation experiment involved tracking the volunteer's movement while sitting in a chair (Figure 5c). As the participant was sitting and leaning back on the chair's backrest, a postural modification of the arms—a swaying motion—was noticeable in every cycle of the test. These observations are reflected in the data acquired by the sensors located on the elbow joints. During these actions, the elbows' flexion and swaying motions resulted in a characteristic double peak in the capacitive signal. Similarly, as the participant leaned forward to stand up, the arms' extension resulted in valley-shaped signals. We also observed that the double peak signals were different in every cycle and the intensity of the signal increased as the motion range increased. Moreover, the sensor's signals for the lower body (i.e., hips and knees) display peak-and-valley signals that can be correlated to the bending of the joints observed during the squat motion (see Video S2, Supporting Information).

The capacitive strain sensors were used to differentiate ranges of human motions during a step-up exercise (Figure 5d). During the step-up movement, the volunteer was asked to place his right foot onto the black box and then bring his left foot up until he was standing on the box with both feet. He was then asked to step down first with the right foot, and then with the left foot so both feet were on the floor. The asynchronous movement of the legs during the step-up movement was distinct in the data acquired by the sensors located in the hips and knees joints. The produced capacitive signal during flexion and extension movements exhibited a multi-peak pattern that was repeatedly observed during all

the cycles of the movement. In addition, the elbow joint-mounted sensors exhibited small but noticeable capacitive responses that reflected the different, subtle swaying motions of the elbow joints during each cycle (see Video S3, Supporting Information).

Characterization of common human motions (e.g., picking up objects from the floor or holding a cup while drinking water) may provide useful information for the treatment of some movement disorders.[76–78] As a demonstration of applicability to these applications, the volunteer was tasked with picking up a paper cup, drinking from it, and finally returning the cup to the floor (Figure 5e). The signals from knee- and hip-mounted sensors displayed a repetitive increase and decrease in capacitance resulting from the successive flexion and extension of the joints during the squat-like movement involved in picking up and returning the object from and to the floor. The elbow joint-mounted sensors also exhibited varying responses matching the different motions of the elbow joints. Overall, the capacitive signal increased with the bending degree of the elbow and returned to its initial value when the arm recovered its initial extended position. Thus, when the left arm is slightly bent during the pick-up movement, the left elbow sensor outputs an increased signal. This increase in capacitance was then followed by a drop to its initial value when the volunteer returned to the standing position and finally, by another slight increase as the volunteer returned the object to the floor. Simultaneously, the right elbow sensor exhibits a three-peak signal, with a first peak corresponding to the arm bending during the pick-up movement. This increase in capacitance, however, is more intense compared to the left elbow because the right arm flexes to a greater degree. The second peak corresponds to the arm flexion during the drinking movement and the third peak results from the slight bending movement of the right arm as the volunteer returns the object to the floor (see Video S4, Supporting Information).

3. Conclusion

In this work, we leverage the characteristics of commonly worn fabric materials to introduce a sensing technology explicitly designed for comfort and long-term functionality in real-world human motion monitoring. The materials and sensor designs presented here serve as a foundation for skin-interfaced wearable sensing technologies, enabling the creation of sensory garments capable of recording physiological movements with high signal fidelity. The air permeability and water vapor transmission properties of the materials used allow the sensor to be highly breathable, which is crucial for maintaining thermophysiological comfort, a characteristic often neglected in wearable systems. Our sensor has not only demonstrated a strain-sensing range, sensitivity, and cyclic performance comparable to other state-of-the-art soft strain sensors, but it also allows for easy integration with commercial activewear, retaining a comfortable clothing-like feel. The easy and low-cost implementation of the fabric sensors in the Arduino environment, as well as the adaptability and customization of the manufacturing process, allows the technology's rapid deployment for the detection of motion of large joints (elbows, hips, and knees) and potentially smaller joints (e.g., finger joints). We further propose a relation to predict the sensor's relative change in capacitance as a function of its elastic properties, dielectric properties, and environmental factors such as temperature and humidity. Future work will focus on the characterization of positional drift and accuracy to enable in situ long-term motion monitoring. Adapted versions of our sensors can bridge the gap between skin-sensor interfacing to facilitate the translation of these technological advances to sports medicine and clinical settings addressing a broad spectrum of conditions, including movement disorders, knee osteoarthritis, and running injuries.

4. Experimental Section

Materials: Medical grade conductive fabric (76% Nylon and 24% elastic fiber, Cat. #A321) was purchased from Less EMF Inc. Nylon 4-way stretch fabric (80% Nylon and 20% Spandex) and stretch cotton jersey fabric (95% Cotton and 5% Spandex) were purchased from Amazon. Polyester-Lycra Spandex fabric (710LY) was purchased from Paylessfabrics. The thermoplastic polyurethane-based adhesive film was produced by Bemis Associates Inc. (3410 Sewfree Tape).

Sensor Fabrication: The sensor electrodes were cut in a dogbone shape (dimensions given in Figure S1, Supporting Information) from the knit conductive fabric using a laser (VLS 3.50, Universal Laser Systems Inc) at 70% intensity and 50% speed. For polyester and nylon dielectric layers, the laser settings were also set at 70% intensity and 50% speed for 2 passes. Cotton was cut with 1 pass with the laser settings at 100% intensity and at 100% speed. The thermoplastic adhesive films used for lamination were laser cut with the adhesive facing up at 90% intensity and 100% speed using 1 pass. Sensors were produced using a stacked assembly method. The three-layer capacitive sensor consists of a pair of conductive electrodes separated by a dielectric layer. First, the dielectric material was laminated with thermoplastic adhesive film on either side (3410 Sewfree Tape), followed by the application of the fabric electrodes on each side of the dielectric. It should be noted that one of the electrodes has a smaller width to prevent shorting of the electrodes. Similarly, for the five-layer sensor, the internal stacked structure consists of one small electrode and two dielectric layers. This assembly was then encased by one big external electrode forming two more layers in the stacked structure (see Figure S1, Supporting Information), with the external electrode connected to ground. All lamination sequences were performed at 160 °C using a heat-press machine for 30 s. The sensors were then interfaced with an LCR meter (E4980AL, Keysight Technologies) using a flexible silicone-sheathed wire (30 AWG) attached to the electrode fabrics (Figure 1). Strain-limiting custom-built tabs made of adhesive laminated woven fabric were attached at each end of the sensor's dogbone shape to facilitate wire interfacing and clamping during the electromechanical tests.

Electromechanical Characterization: Each tested specimen was cyclically pre-stretched 10 times to 100% strain (original stretchable gauge length, $L_0 = 106 \pm 2$ mm) to remove the Mullins effect and achieve a fixed level of plastic deformation. After the pre-stretching cycles, the new stretchable length of the specimens was registered as the new gauge length. Sensors were then stretched to their original stretchable length (106 ± 2 mm), which was approximately 82%–88% strain of the new registered L_0, at a rate of 5 *mm/s* using the materials testing system (Instron 3345).

The capacitance of the sensors was recorded with the LCR meter (E4980AL, Keysight Technologies) at an excitation frequency of 1 kHz. The measured capacitance was adjusted to represent only the capacitance of the stretchable area by subtracting the capacitance of the stationary tab areas from the LCR measurements. The capacitance of the tab areas was calculated as a percentage of the initial capacitance C_0 using the relative size of the tab areas reported in Figure S1 (Supporting Information).

Excluding the three-layer cotton sensors, the averaged response of five sensors was shown for each dielectric material and sensor configuration (three- or five-layer). For the three-layer cotton sensors, the averaged response of three sensors was shown due to sensor shorting during testing. The bands shown represent the standard deviations of the averaged responses from all the tested sensors. Unless otherwise noted,

all electromechanical characterizations of the sensors were performed at a temperature of 24 ± 1°C and relative humidity of 51 ± 3%.

Dynamic electromechanical characterization of the sensors was carried out through 5000 cycles of straining up to 60% using a custom-built cyclic tester, as described by Porte and co-authors.[36] For cyclic testing, representative data from one sensor was selected for each dielectric material and sensor configuration.

Sensor frequency sweep testing was performed using the frequency sweep function of an LCR meter (Keysight E4980A/AL). The excitation frequency ranged from 20 Hz to 1 MHz. Measurements were performed while the sensor was stationary at 0% and 55% strain and averaged for five sensors.

Humidity and temperature dependence of the sensors' electromechanical properties were investigated with a materials testing system (Instron 3345) equipped with a custom-built environmental chamber (Model 5500 - 8485, ETS). For humidity tests, the sensors were left inside the environmental chamber for at least 3 h prior to testing and an average response of five sensors of each type was shown. Subsequent testing was performed at 90 ± 2% RH, and two different temperatures, 35 and 25 °C, to simulate sweating conditions.

Materials Characterization: The morphology of the fabrics was investigated using a scanning electron microscope Hitachi SU8230 UHR cold field emission. Air permeability of the bare and laminated fabric samples was measured according to the standard test method for textile fabrics (ASTM D737), using an air permeability tester (SDL Atlas MO21A) with a test area of 20 cm^2 and at a constant pressure drop of 200 Pa. Laminated fabric samples were tested with the adhesive film against the bottom plate. The water vapor transmission rate (WVTR) was determined according to the standard test (ASTM E 96), using a WVTR Analyzer (Mocon AQUATRAN 3) with a cup diameter of 2.5 inches. Samples undergoing air permeability and WVTR tests were pre-conditioned at a temperature of 21 ± 1° C and a relative humidity of 65 ± 2% according to the standard described in ASTM D1776. The thickness of fabric samples was measured using a parallel presser digital caliper. Photographic images of the fabrics were captured using a handheld USB digital microscope with LED illumination (plugable UTP200X020MP). All measurements were repeated three times.

Washability: The washing test of the sensors was conducted at room temperature by diluting 3 mL of a commercial neutral detergent (TexCare, #A289-L) into 1000 mL of deionized (DI) water at a pH 6, and the subsequent continuous stirring for 30 min. After this, the textile sensors were rinsed with DI water and dried overnight in an oven at 60°C followed by a conditioning step at a temperature of 24 ± 1°C and relative humidity of 51 ± 3%. The washing procedure was conducted three times. The electromechanical properties of the washed sensors were monitored after each washing-drying cycle. For each dielectric material, the electromechanical response was reported as an average of five sensors.

Manufacturing of Conformable Sensory Bodysuit and Data Acquisition: A sensory bodysuit was manufactured to characterize integration and performance at the human-sensor interface. Commercial form-fitting garments were utilized to manufacture the sensory bodysuit consisting of a men's compression long-sleeve T-shirt (Under Armour) and a pair of men's leggings (Willit sports). Six sensors with the same dogbone shape were heat pressed into the garments, with the garment's fabric serving as one of the dielectric layers of the five-layer sensor structure (see Figure S1, Supporting Information). With the exception of the garment fabric, all other layers of the sensors were cut using the same laser settings described in §4.2. First, fabric electrodes were interfaced with flexible silicone-sheathed wire (30 AWG) before the sensor construction. The garment was then laminated with thermoplastic adhesive (3410 Sewfree Tape), followed by the application of the inner fabric electrode. Then, a second dielectric layer was stacked and attached with the same thermoplastic adhesive. After this, a small slit was cut in the garment to wrap the larger external electrode around the sensor, forming the last two layers in the five-layer sensor (see Figure S1, Supporting Information). Finally, strain-limiting custom-built tabs made of adhesive laminated woven fabric were attached at each end of the sensor's dogbone shape to facilitate wire interfacing and to cover the slit made in the garment in the previous step. All manufacturing sequences were performed at 160 °C using a heat-press machine for 30 s. The sensors were positioned at the major joints—elbows, knees, and hips—to detect the motion of the upper and lower limbs. No additional calibration process or manufacturing adjustments were required to achieve the sensor responses shown in these demonstrations. The agreements between each pair of sensors on the same type of joint were achieved on the first attempt of sensor integration and testing. The change in capacitance versus time was measured using a commercial capacitive sensor breakout board (MPR121, Adafruit) and an Arduino Pro mini using the CoolTerm application for data acquisition.

Supporting Information

Supporting Information is available from the Wiley Online Library or from the author.

Acknowledgements

L.S.-B. and A.A. contributed equally to this work. The authors thank Prof. Holly Yanco and Cheryl A. Gomes, with the Fabric Discovery Center at UMass Lowell, for their assistance in collecting permeability data; Min Li from the west campus materials characterization core at Yale University for access to characterization equipment; and Dr. Dylan Shah and Dr. Elze Porte for valuable discussions regarding the capacitive sensors and applications of this work. This material was based upon work supported by the NSF under grant no. IIS-1954591. The study received IRB approval (Protocol ID 2000031654, approved by the Human Investigation Committee 2B with the Yale Human Research Protection Program) and appropriate guidelines were followed. The proof-of-concept demonstrations included in this work were conducted in accordance with the ethical principles of the Declaration of Helsinki. Informed consent for participation and publication was obtained from the volunteer.

Conflict of Interest

The authors have declared no conflict of interest.

Data Availability Statement

The data that support the findings of this study are available from the corresponding author upon reasonable request.

Keywords

fabric sensors, soft robotics, soft sensors, textile sensors, wearable electronics

Received: March 9, 2023
Revised: May 15, 2023
Published online: July 7, 2023

[1] P. Nogueira, J. Urbano, L. P. Reis, H. L. Cardoso, D. C. Silva, A. P. Rocha, J. Gonçalves, B. M. Faria, *J. Med. Syst.* **2018**, *42*, 101.
[2] V. G. Motti, in *Wearable Interaction*, Springer, Berlin, **2020**.
[3] M. Amjadi, A. Pichitpajongkit, S. Lee, S. Ryu, I. Park, *ACS Nano* **2014**, *8*, 5154.
[4] S. Patel, H. Park, P. Bonato, L. Chan, M. Rodgers, *J. Neuroeng. Rehabil.* **2012**, *9*, 21.
[5] E. Mencarini, A. Rapp, L. Tirabeni, M. Zancanaro, *IEEE Trans. Hum. Mach. Syst.* **2019**, *49*, 314.

[6] S. Coyle, D. Morris, K. T. Lau, D. Diamond, N. Moyna, in *Proc. IEEE 6th Int. Workshop on Wearable and Implantable Body Sensor Networks*, Berkeley, CA, USA **2009**, pp. 307.
[7] K. Guk, G. Han, J. Lim, K. Jeong, T. Kang, E. K. Lim, J. Jung, *Nanomaterials* **2019**, *9*, 813.
[8] S. M. De Rossi, N. Vitiello, T. Lenzi, R. Ronsse, B. Koopman, A. Persichetti, F. Giovacchini, F. Vecchi, A. J. Ijspeert, H. van der Kooij, M. C. Carrozza, in IEEE Annual International Conference of the IEEE Engineering in Medicine and Biology, **2010**, p. 1279.
[9] B. R. Hindle, J. W. Keogh, A. V. Lorimer, *Appl. Bionics Biomech.* **2021**, *2021*, 6628320.
[10] D. Kim, J. Kwon, S. Han, Y. L. Park, S. Jo, *IEEE/ASME Trans. Mechatron.* **2019**, *24*, 56.
[11] G. B. Guerra-Filho, *Rev. Inform. Teor. Apl.* **2005**, *12*, 61.
[12] J. Taborri, J. Keogh, A. Kos, A. Santuz, A. Umek, C. Urbanczyk, E. van der Kruk, S. Rossi, *Appl. Bionics Biomech.* **2020**, *2020*, 2041549.
[13] E. van der Kruk M. M. Reijne, *Eur. J. Sport Sci.* **2018**, *18*, 806.
[14] J. Shintake, E. Piskarev, S. H. Jeong, D. Floreano, *Adv. Mater. Technol.* **2018**, *3*, 1700284.
[15] W. Yi, Y. Wang, G. Wang, X. Tao, *Polym. Test.* **2012**, *31*, 677.
[16] M. Nankali, N. M. Nouri, M. Navidbakhsh, N. G. Malek, M. A. Amindehghan, A. M. Shahtoori, M. Karimi, M. Amjadi, *J. Mater. Chem. C* **2020**, *8*, 6185.
[17] X. Hu, F. Yang, M. Wu, Y. Sui, D. Guo, M. Li, Z. Kang, J. Sun, J. Liu, *Adv. Mater. Technol.* **2022**, *7*, 2100769
[18] C. Choi, J. M. Lee, S. H. Kim, S. J. Kim, J. Di, R. H. Baughman, *Nano Lett.* **2016**, *16*, 7677.
[19] J. Lee, S. Kim, J. Lee, D. Yang, B. C. Park, S. Ryu, I. Park, *Nanoscale* **2014**, *6*, 11932.
[20] Y. Yang, S. Duan, W. Xiao, H. Zhao, *Sens. Actuators, A* **2022**, *343*, 113653.
[21] J. Li, G. Zhang, R. Sun, C. P. Wong, in *Three-Dimensional Graphene-Based Composite for Elastic Strain Sensor Applications*, Cambridge University Press, Cambridge, Vol. *1*, **2016**, pp. 2415–2420.
[22] H. R. Na, H. J. Lee, J. H. Jeon, H. J. Kim, S. K. Jerng, S. B. Roy, S. H. Chun, S. Lee, Y. J. Yun, *npj Flexible Electron.* **2022**, *6*, 2.
[23] Y. Wu, Y. Zhou, W. Asghar, Y. Liu, F. Li, D. Sun, C. Hu, Z. Wu, J. Shang, Z. Yu, R.-W. Li, H. Yang, *Adv. Intell. Syst.* **2021**, *3*, 2000235.
[24] D. Zhang, J. Zhang, Y. Wu, X. Xiong, J. Yang, M. D. Dickey, *Adv. Intell. Syst.* **2022**, *4*, 2100201.
[25] J. Chen, J. Zhang, Z. Luo, J. Zhang, L. Li, Y. Su, X. Gao, Y. Li, W. Tang, C. Cao, Q. Liu, L. Wang, H. Li, *ACS Appl. Mater. Interfaces* **2020**, *12*, 22200.
[26] C. B. Cooper, K. Arutselvan, Y. Liu, D. Armstrong, Y. Lin, M. R. Khan, J. Genzer, M. D. Dickey, *Adv. Funct. Mater.* **2017**, *27*, 1605630.
[27] A. Frutiger, J. T. Muth, D. M. Vogt, Y. Mengüç, A. Campo, A. D. Valentine, C. J. Walsh, J. A. Lewis, *Adv. Mater.* **2015**, *27*, 2440.
[28] D. Y. Choi, M. H. Kim, Y. S. Oh, S. H. Jung, J. H. Jung, H. J. Sung, H. W. Lee, H. M. Lee, *ACS Appl. Mater. Interfaces* **2017**, *9*, 1770.
[29] M. Amjadi, K. U. Kyung, I. Park, M. Sitti, *Adv. Funct. Mater.* **2016**, *26*, 1678.
[30] T. Yamada, Y. Hayamizu, Y. Yamamoto, Y. Yomogida, A. Izadi-Najafabadi, D. N. Futaba, K. Hata, *Nat. Nanotechnol.* **2011**, *6*, 296.
[31] C. Shi, Z. Zou, Z. Lei, P. Zhu, G. Nie, W. Zhang, J. Xiao, *Research* **2021**, *2021*, 9846036.
[32] H. Souri, H. Banerjee, A. Jusufi, N. Radacsi, A. A. Stokes, I. Park, M. Sitti, M. Amjadi, *Adv. Intell. Syst.* **2020**, *2*, 2000039.
[33] S. Seyedin, P. Zhang, M. Naebe, S. Qin, J. Chen, X. Wang, J. M. Razal, *Mater. Horiz.* **2019**, *6*, 219.
[34] S. Z. Homayounfar T. L. Andrew, *SLAS Technol.* **2020**, *25*, 9.
[35] E. L. White, M. C. Yuen, J. C. Case, R. K. Kramer, *Adv. Mater. Technol.* **2017**, *2*, 1700072.
[36] E. Porte, T. Sipple, L. S. Botero, D. Shah, R. Kramer-Bottiglio, in *2021 IEEE 4th Int. Conf. on Soft Robot., RoboSoft 2021*, New Haven, CT, USA **2021**, 412.
[37] R. A. Bilodeau, A. M. Nasab, D. S. Shah, R. Kramer-Bottiglio, *Soft Matter* **2020**, *16*, 5827.
[38] A. Atalay, V. Sanchez, O. Atalay, D. M. Vogt, F. Haufe, R. J. Wood, C. J. Walsh, *Adv. Mater. Technol.* **2017**, *2*, 1700136.
[39] H. Park, J. Cho, J. Park, Y. Na, J. Kim, *IEEE Rob. Autom. Lett.* **2020**, *5*, 3525.
[40] Y. Mengüç, Y. L. Park, E. Martinez-Villalpando, P. Aubin, M. Zisook, L. Stirling, R. J. Wood, C. J. Walsh, in *Proc. IEEE Int. Conf. on Robot. and Autom.*, IEEE, Piscataway, NJ, USA **2013**, 5309.
[41] Y. Mengüç, Y. L. Park, H. Pei, D. Vogt, P. M. Aubin, E. Winchell, L. Fluke, L. Stirling, R. J. Wood, C. J. Walsh, *Int. J. Rob. Res.* **2014**, *33*, 1748.
[42] E. T. Özkan B. Meriç, *Text. Res. J.* **2015**, *85*, 62.
[43] A. S. for Testing M. (ASTM), D737-18, standard test method for air permeability of textile fabrics.
[44] R. P. Jamdagni, S. Bhattacharya, N. Kumar, *ACC J.* **2015**, *21*, 54.
[45] B. Das, A. Das, V. K. Kothari, R. Fangueiro, M. de Araújo, *J. Text. Inst.* **2009**, *100*, 588.
[46] D. Y. Limeneh, M. Ayele, T. Tesfaye, E. Z. Liyew, A. F. Tesema, *J. Nat. Fibers* **2020**, *19*, 4148.
[47] A. Bivainytė, D. Mikučionienė,*Fibres Text. East. Eur.* **2011**, *19*, 69.
[48] B. Wilbik-Hałgas, R. Danych, B. Wiecek, K. Kowalski, *Fibres Text. East. Eur.* **2006**, *14*, 77.
[49] E. Onofrei, A. M. Rocha, A. Catarino, *J. Eng. Fibers Fabr.* **2011**, *6*, 10.
[50] C. Prahsarn, R. L. Barker, B. S. Gupta, *Text. Res. J.* **2005**, *75*, 346.
[51] K. K. Kim, I. H. Ha, M. Kim, J. Choi, P. Won, S. Jo, S. H. Ko, *Nat. Commun.* **2020**, *11*, 2149.
[52] G. Havenith H. O. Nilsson, *Eur. J. Appl. Physiol.* **2004**, *92*, 636.
[53] M. Cao, Y. Li, Y. Guo, L. Yao, Z. Pan, *IEEE Comput. Graphics Appl.* **2016**, *36*, 70.
[54] L. Tian, B. Zimmerman, A. Akhtar, K. J. Yu, M. Moore, J. Wu, R. J. Larsen, J. W. Lee, J. Li, Y. Liu, B. Metzger, S. Qu, X. Guo, K. E. Mathewson, J. A. Fan, J. Cornman, M. Fatina, Z. Xie, Y. Ma, J. Zhang, Y. Zhang, F. Dolcos, M. Fabiani, G. Gratton, T. Bretl, L. J. Hargrove, P. V. Braun, Y. Huang, J. A. Rogers, *Nat. Biomed. Eng.* **2019**, *3*, 194.
[55] M. Seok, S. Yoon, M. Kim, Y. H. Cho, *Nanoscale Adv.* **2021**, *3*, 4843.
[56] V. Kumar, V. R. Sampath, C. Prakash, *J. Text. Inst.* **2016**, *107*, 1213.
[57] G. Dusserre, L. Balea, G. Bernhart, *Composites, Part A* **2014**, *64*, 185.
[58] E. Porte, R. Kramer-Bottiglio, *Adv. Mater. Technol.* **2021**, *6*, 2001247.
[59] Z. Laufer, Y. Diamant, M. Gill, G. Fortuna, *Int. J. Polym. Mater. Polym. Biomater.* **1978**, *6*, 159.
[60] S. C. Mannsfeld, B. C. Tee, R. M. Stoltenberg, C. V. Chen, S. Barman, B. V. Muir, A. N. Sokolov, C. Reese, Z. Bao, *Nat. Mater.* **2010**, *9*, 859.
[61] L. Ma, X. Shuai, Y. Hu, X. Liang, P. Zhu, R. Sun, C. P. Wong, *J. Mater. Chem. C* **2018**, *6*, 13232.
[62] Z. He, W. Chen, B. Liang, C. Liu, L. Yang, D. Lu, Z. Mo, H. Zhu, Z. Tang, X. Gui, *ACS Appl. Mater. Interfaces* **2018**, *10*, 12816.
[63] W. Geng, T. J. Cuthbert, C. Menon, *ACS Appl. Polym. Mater.* **2021**, *3*, 122.
[64] Y. Yamada, *Textiles* **2022**, *2*, 50.
[65] S. R. A. Ruth Z. Bao, *ACS Appl. Mater. Interfaces* **2020**, *12*, 58301.
[66] A. Yoshida, Y.-F. Wang, T. Sekine, Y. Takeda, D. Kumaki, S. Tokito, *ACS Appl. Energy Mater.* **2022**, *14*, 5721.
[67] H. Nakamoto, H. Ootaka, M. Tada, I. Hirata, F. Kobayashi, F. Kojima, *IEEE Sens. J.* **2015**, *15*, 2212.
[68] J. C. Case, E. L. White, R. K. Kramer, *Soft Rob.* **2015**, *2*, 80.
[69] M. E. Messiry A. Mohamed, *J. Text. Inst.* **2016**, *107*, 431.
[70] T. Igarashi, M. Hoshi, K. Nakamura, T. Kaharu, K. I. Murata, *J. Phys. Chem. C* **2020**, *124*, 4196.
[71] S. Yagihara, H. Saito, H. Sugimoto, T. Kawaguchi, M. Fukuzaki, T. Igarashi, M. Hoshi, K. Nakamura, *Asian J. Mater. Sci.* **2021**, *56*, 17844.

[72] E. Jayamani, S. Hamdan, M. R. Rahman, M. K. B. Bakri, *Procedia Eng.* **2014**, *97*, 536.
[73] R. Salvado, C. Loss, Gon, P. Pinho, *Sensors* **2012**, *12*, 15841.
[74] C. L. Ng M. B. I. Reaz, *Sensors* **2017**, *17*, 574.
[75] S. Ahmad, K. Subhani, A. Rasheed, M. Ashraf, A. Afzal, B. Ramzan, Z. Sarwar, *J. Electron. Mater.* **2020**, *49*, 1330.
[76] N. Jalloul, *Biomed. J.* **2018**, *41*, 249.
[77] M. Pau, S. Caggiari, A. Mura, F. Corona, B. Leban, G. Coghe, L. Lorefice, M. G. Marrosu, E. Cocco, *Mult. Scler. Relat. Disord.* **2016**, *10*, 187.
[78] I. Carpinella, D. Cattaneo, G. Bonora, T. Bowman, L. Martina, A. Montesano, M. Ferrarin, *Arch. Phys. Med. Rehabil.* **2017**, *98*, 622.